Dependence of Domain-Wall Depinning Threshold Current on Pinning Profile

S. Lepadatu,[1,*] A. Vanhaverbeke,[2] D. Atkinson,[3] R. Allenspach,[2] and C. H. Marrows[1,†]

[1]*School of Physics and Astronomy, E. C. Stoner Laboratory, University of Leeds, Leeds LS2 9JT, United Kingdom*
[2]*IBM Research, Zurich Research Laboratory, CH-8803 Rüschlikon, Switzerland*
[3]*Department of Physics, Science Laboratories, University of Durham, Durham DH1 3LE, United Kingdom*

(Received 26 November 2007; published 26 March 2009)

We have investigated the threshold current density required for depinning a domain wall from constrictions in NiFe nanowires, which give rise to pinning potentials of fixed amplitude but variable profile. We observed it to vary linearly with the angle of the triangular constriction. These results are reproduced using micromagnetic simulations including the adiabatic and nonadiabatic spin-torque terms. By curve-fitting the calculated variations to the experimental results, we obtain the nonadiabaticity parameter $\beta = 0.04(\pm 0.005)$ and current spin polarization $P = 0.51(\pm 0.02)$.

DOI: 10.1103/PhysRevLett.102.127203 PACS numbers: 75.60.Ch, 72.25.Ba, 72.25.Pn

The topic of current-induced domain-wall (DW) movement [1] has seen growing interest in recent years not only due to its promising applications to spintronics devices, such as magnetic logic gates and magnetic random access memory, but also due to the fascinating underlying physics. Experimental work on this subject includes studies on ferromagnetic thin films [2,3], nanowires [4–8], and wires with patterned pinning sites [9–13]. In addition to the early theoretical work [14,15], recent reformulations have been proposed, based on a microscopic approach [16–19]. A key issue is the dependence of the threshold current for DW movement on the details of the pinning potential. As shown by Tatara and Kohno [16], in the limit of thick DWs and weak pinning, the threshold current is expected to be proportional to the transverse anisotropy $K_\perp$. This has been demonstrated recently in NiFe wires where the threshold current was measured as a function of hard-axis anisotropy by varying the aspect ratio of the wires [20]. On the other hand, in the limit of thin walls and/or strong pinning, the threshold current is expected to depend on the strength of the pinning potential [16]. This latter conclusion has been verified experimentally by Ravelosona *et al.* [21] in spin valve structures having perpendicular magnetic anisotropy, showing a strong dependence of the threshold current on pinning potential depth. In this work we investigate the variation of threshold current in single-layer wires patterned with a notch pinning site, as a function of the notch angle. Hence we hold the depth of the pinning potential constant while studying the effect of its profile and observe a linear variation of the threshold current with angle. Thus, by engineering the geometry of the pinning profile we demonstrate control of the depinning properties of DWs.

A set of notched structures, shown in Fig. 1(a), has been fabricated on Si/SiO_2 substrates using *e*-beam lithography and sputtering of $Ni_{80}Fe_{20}$(20 nm)/Au(1 nm). The wire width and constriction width are kept fixed at 1.4 μm and 500 nm, respectively, while the notch angle θ, defined as the angle at the tip of the constriction triangle pointing towards the center of the constriction, is varied from 21° up to 53°. A two-point measurement setup was used as shown in the inset in Fig. 1(b) with Ta(10 nm)/Au(190 nm) measurement leads. The magnetization switching properties of these structures were investigated at room temperature using magnetoresistance (MR) and focused magneto-optical Kerr effect (MOKE) measurements.

A typical longitudinal MR measurement is shown in Fig. 1(b), where the magnetic field is applied along the length of the wire. Here the MR loop is measured using a lock-in amplifier detection method with a sinusoidal excitation current of 10 μA amplitude and 10 kHz frequency. The MR measurement on the right-hand side of Fig. 1(b) is obtained following saturation in a −2 kOe field, and similarly the measurement on the left-hand side is obtained

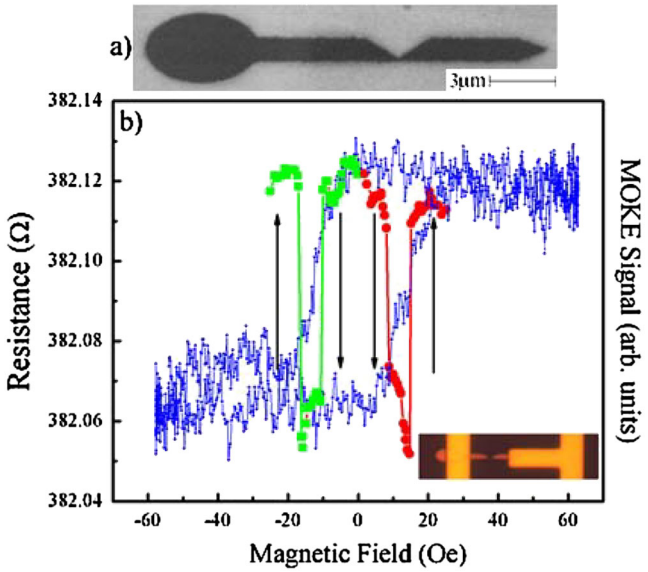

FIG. 1 (color online). (a) SEM image (uncontacted), and (b) longitudinal MR measurement (large circles and squares) and focused MOKE measurement (small circles) of a structure with a 43.1° notch angle. The inset shows a wire with the contact pads used for measurements.

following saturation in a +2 kOe field. The elliptical pad shown in Fig. 1(a) has a coercivity of around 10 Oe, and this is used to nucleate DWs which propagate along the wire and are pinned at the constriction, while the pointed end suppresses DW formation at the other end of the wire [22]. After reversal from saturation, a sharp drop in resistance is observed at 10 Oe in Fig. 1(b) due to the anisotropic MR (AMR) contribution of a DW trapped at the constriction. Increasing the magnitude of the magnetic field further, the resistance gradually decreases until a sharp rise in resistance is observed at around 15 Oe. The gradual decrease in resistance may be understood as the additional AMR contribution due to the displacement of the DW from the center of the constriction [23], while the sharp rise in resistance occurs due to DW depinning. The magnetization switching mechanism was also investigated using focused MOKE measurements, as shown in Fig. 1(b), where the laser spot, with a diameter of 5 μm, was centered on the constriction and the measurements were obtained by averaging over many single MOKE loops. This can lead to some broadening due to averaging of stochastic variations of the switching field. Taking into account the signal to noise ratio on the data, the MOKE measurements show switching steps that are correlated in field with those obtained from MR measurement. The good match between the MOKE and MR measurements confirms the magnetization switching mechanism. The symmetry of the curves indicates no differences in depinning for head-to-head or tail-to-tail walls.

The MR measurement shown in Fig. 1(b) is repeated for the different notch structures by varying the direct current (dc) offset. In Fig. 2(a), the measurement for the structure with a 43° notch angle is shown, where the dc offset is changed in 10 μA steps. The resistance values are color coded, the scale ranging from red (lowest resistance) up to blue (highest resistance). To take account of the Joule heating of the wires which causes a monotonic increase in the measured resistance with dc offset, the MR loops used in Fig. 2(a) are normalized to the highest percentage change. The overall change in resistance for a DW is about 0.06 Ω, which is a factor of 5 smaller than suggested by numerical modeling [24], and we estimate a corresponding increase in sample temperature of around 14 K [25]. The red bands are due to DW formation at the constriction ($\pm$10 Oe) and subsequent depinning ($\pm$15 Oe). Here the positive current corresponds to electron flow from the left to the right (from the ellipse to the pointed end). Increasing the dc offset beyond +1.2 mA suppresses DW pinning at the constriction for both negative and positive magnetic fields. For the constriction width of 500 nm, this dc offset corresponds to a current density of $\sim 10^{11}$ A/m^2. This behavior is not symmetrical with reversal of current direction, confirming that the suppression of DW pinning is due to the spin-polarized current acting on the wall, which augments the effect of the field [2,15]. We can rule out the Joule heating effect as the cause of DW pinning suppression since that effect is independent of the current direction. Moreover, there is no smooth monotonic change in the depinning field as a function of current magnitude which would indicate the influence of heating.

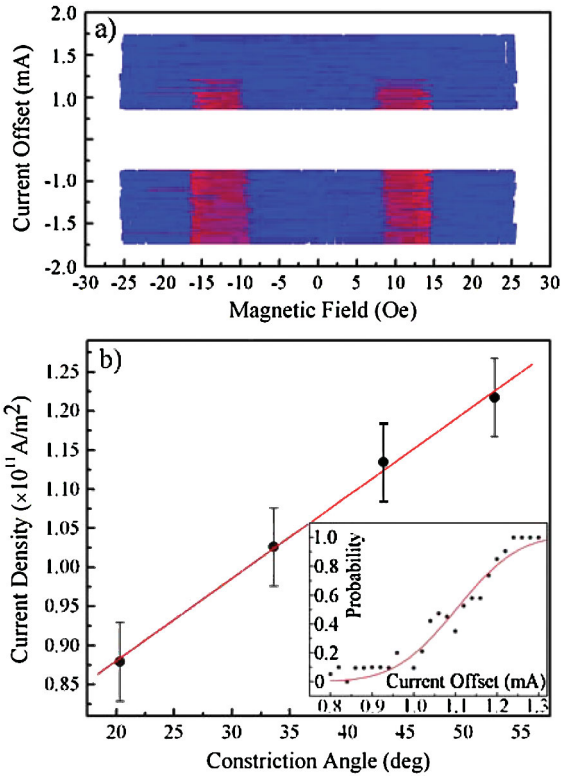

FIG. 2 (color). (a) Longitudinal MR response as a function of dc offset for a notch angle of 43°, where the positive field data are MR sweeps following saturation in the −2 kOe field and the negative field data are MR sweeps following saturation in the +2 kOe field. (b) Mean threshold current density at a longitudinal field of 10 Oe versus notch angle where the solid circles are the experimental points, together with the associated error bars due to uncertainties in device dimensions, and the line is a straight line fit. In the inset, the probability of DW depinning as a function of dc offset is shown for the notch angle of 43°, where the solid circles are the experimental points and the solid curve is an error function fit.

To determine the mean threshold current, the probability of DW depinning as a function of dc offset is obtained using the following procedure. At zero dc offset, a DW is pinned at the constriction, detected by measurement of the device resistance. Following successful wall pinning, a given dc offset is applied for 1 s at a longitudinal field of 10 Oe, following which the dc offset is reduced to zero and DW depinning is tested by further increasing the field and measuring any resulting resistance change. For each dc offset value, this procedure is repeated 20 times to obtain the probability of DW depinning, and the result obtained for the 43° notch angle is shown in the inset in Fig. 2(b). The probability distribution of DW depinning as a function of dc offset arises due to thermal activation processes [26–29] described by a Gaussian probability function. The measurement shown in the inset in Fig. 2(b) represents

the cumulative distribution function of this process Φ, and by curve-fitting the measured points using the cumulative Gaussian function

$$\Phi = \frac{1}{2}\left[1 + \mathrm{erf}\left(\frac{x-\mu}{\sigma\sqrt{2}}\right)\right], \quad (1)$$

the mean threshold current value μ and standard deviation σ are obtained. The value thus obtained is found to be in agreement with the measurement shown in Fig. 2(a). By repeating the same procedure for the samples with different angle θ, the dependence of the mean threshold current density on θ is obtained as shown in Fig. 2(b). In all cases, the standard deviation was found to be around 130 μA. The mean threshold current density J_C is found to vary linearly with the notch angle θ in the range 20°–55°, according to

$$J_C = a + b\theta, \quad (2)$$

where $a = 6.7 \times 10^{10}$ A/m^2 and $b = 1.06 \times 10^9$ A/m^2 per degree.

The threshold current was also measured as a function of notch angle using pulsed current (pc), allowing measurements in zero field due to much reduced Joule heating. By using a pulse width of 380 ns, the threshold current is determined both in zero field and with a longitudinal magnetic field of 10 Oe using the following procedure: (i) A DW is pinned at the constriction using a 10 Oe reversal field. (ii) The measurement field is set, and a single voltage pulse of given amplitude is applied to the sample. The pulse polarity is selected so that the resulting spin torque acts in the same direction as the magnetic field—electrons flowing from left to right in Fig. 1(a). (iii) The depinning of the DW is tested by increasing the magnetic field past the depinning field value and measuring the resulting resistance change. This procedure is repeated 5 times for each pulse amplitude to obtain the distribution of depinning probability with pulse amplitude. For the samples investigated here, the transmission coefficient was measured to be around 0.4, and, together with the cross-sectional area at the constriction, the pulse amplitude values are converted into current density values. By using Eq. (1), the mean threshold current density is obtained as described above. These results are summarized in Fig. 4(a), together with the results obtained from dc measurements. The variation of threshold current with notch angle is again found to be linear for both 0 and 10 Oe fields, again described by Eq. (2), where the values of a and b are listed in Table I.

The main difference between the pc and dc measurements at the 10 Oe field is expected to be due to the Joule heating associated with the dc offsets, compared to the pc measurements, resulting in decreased threshold currents. Thus, when numerically comparing the experimental results with micromagnetic simulations, it is important to consider the pc measurements alone. As expected, the pc measurements at 10 Oe show much smaller threshold currents compared to those at 0 Oe due to the decreased effective pinning potential.

TABLE I. Coefficients a and b for Eq. (2) for the different measurement types.

Measurement type	$a(10^{11}$ A/m$^2)$	$b(10^9$ A/m^2 degree)
Pulses 0 Oe	7.8 ± 0.1	0.9 ± 0.2
Pulses 10 Oe	2.2 ± 0.1	1.4 ± 0.2
dc 10 Oe	0.7 ± 0.1	1.1 ± 0.2

In order to calculate the threshold current as a function of notch angle, micromagnetic simulations have been performed using a modified version of the object oriented micromagnetic framework (OOMMF) software [30], with the Landau-Lifshitz-Gilbert equation including both the adiabatic and nonadiabatic spin-torque terms as shown in Eq. (3) [17,19], with parameters characteristic of $Ni_{80}Fe_{20}$, namely, saturation magnetization $M_s = 8.6 \times 10^5$ A/m, exchange stiffness $A = 1.3 \times 10^{-11}$ J/m, and cell size of 5 nm:

$$\frac{\partial \mathbf{m}}{\partial t} = \gamma \mathbf{H}_{\mathrm{eff}} \times \mathbf{m} + \alpha \mathbf{m} \times \frac{\partial \mathbf{m}}{\partial t} - u\frac{\partial \mathbf{m}}{\partial x} + \beta u \mathbf{m} \times \frac{\partial \mathbf{m}}{\partial x}. \quad (3)$$

Here γ is the gyromagnetic ratio, α is the damping constant, and $u = JPg\mu_B/2eM_S$, where J is the charge current density and P is the current spin polarization. The last two terms on the right-hand side of Eq. (3) are, in order, the adiabatic and nonadiabatic spin-torque terms. The contribution of the latter term is determined by the nonadiabaticity parameter β, given by $\beta = \hbar/J_{\mathrm{ex}}\tau_{\mathrm{sf}}$ [19], where J_{ex} is the s-d exchange interaction energy and τ_{sf} is the spin-flip time. In order to obtain the starting state for these simulations, namely, the DW pinning position, spin scanning electron microscope (SEM) [31] images were ob-

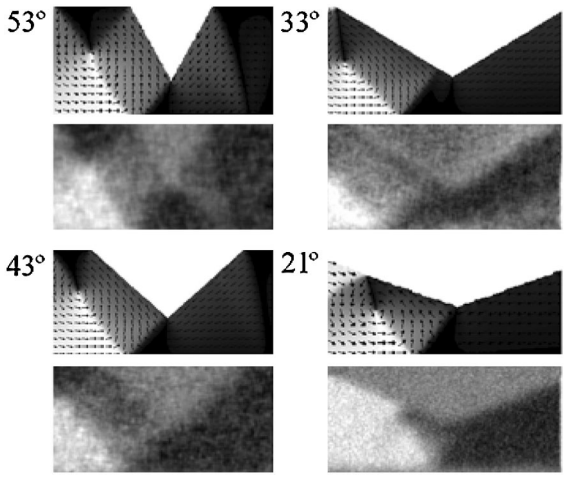

FIG. 3. DW pinning position at zero magnetic field, after reversal from saturation, as a function of notch angle determined using micromagnetic simulations (top) and spin-SEM imaging (bottom). The spin-SEM images show the magnetization direction along the length of the wire.

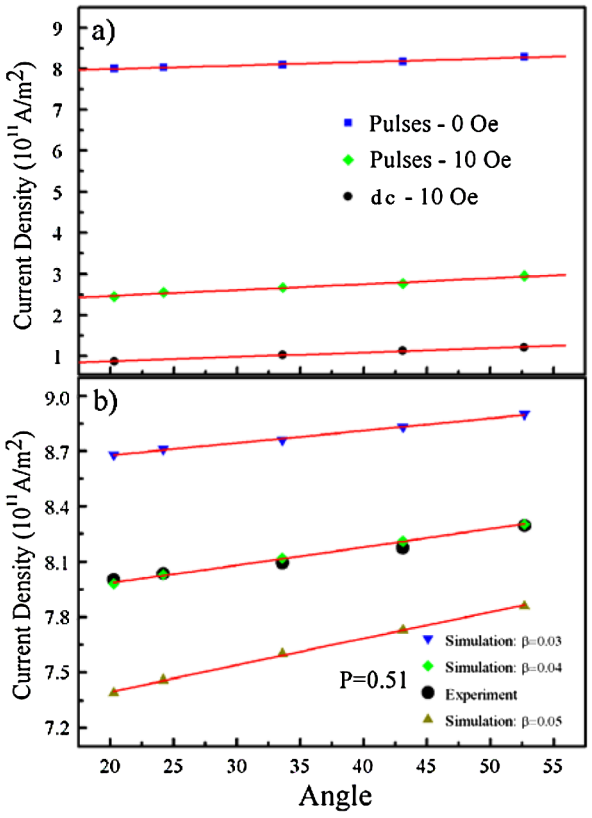

FIG. 4 (color online). (a) Summary of experimental results showing variation of threshold current with notch angle. (b) Calculated threshold current as a function of notch angle at 0 Oe for nonadiabaticity parameter β of 0.03, 0.04, and 0.05 and best fit current spin polarization P of 0.51. The solid circles are the threshold current values measured at 0 Oe using pc measurements.

tained at zero field after DW pinning for each notch angle. The DW pinning mechanism has also been reproduced using micromagnetic simulations on the geometry of the measured wires, using a 10 Oe reversal field. The final DW pinning position is obtained at zero field, and these are shown in Fig. 3 together with the DW configuration obtained from spin-SEM imaging. We find excellent agreement between the spin-SEM imaging and micromagnetic simulations for the DW pinning position for each notch angle.

From the starting state, for a fixed value of β the threshold value of u is calculated using the stopping condition $|M \times H|/|\mathbf{M} \times \mathbf{S}|^2 < 10^{-5}$. For $Ni_{80}Fe_{20}$ we have $u = JP \times 7.24 \times 10^{-11}$, $\alpha = 0.02$ [19], and for each value of β the current spin polarization P is varied to obtain the best fit to the experimental results. In Fig. 4(b), the calculated variations of threshold current with notch angle are shown for the case of 0 Oe, where the best fit is obtained for $\beta = 0.04(\pm 0.005)$ and $P = 0.51(\pm 0.02)$. The calculated variation of the threshold current as a function of notch angle is again found to be linear, in agreement with the experimental results. We also find that the slope of this linear relation increases with the nonadiabaticity parameter β, thus allowing for β to be determined by curve-fitting the calculated threshold current variations to the experimental results.

In conclusion, we have measured the depinning threshold current for notched structures as a function of notch angle and observed it to vary linearly with notch angle. These results are reproduced using micromagnetic simulations including the adiabatic and nonadiabatic spin-torque terms, and, by curve-fitting the calculated variations to the experimental results, we obtain the values $\beta = 0.04(\pm 0.005)$ and $P = 0.51(\pm 0.02)$.

We acknowledge useful discussions with Gen Tatara. This research was supported by the ESF EUROCORES collaborative research project SpinCurrent under the Fundamentals of Nanoelectronics program and by the EPSRC through the Spin@RT consortium.

*s.lepadatu@leeds.ac.uk
†c.h.marrows@leeds.ac.uk

[1] C. H. Marrows, Adv. Phys. **54**, 585 (2005).
[2] L. Gan *et al.*, IEEE Trans. Magn. **36**, 3047 (2000).
[3] P. P. Freitas and L. Berger, J. Appl. Phys. **57**, 1266 (1985).
[4] N. Vernier *et al.*, Europhys. Lett. **65**, 526 (2004).
[5] A. Yamaguchi *et al.*, Phys. Rev. Lett. **92**, 077205 (2004).
[6] E. Saitoh *et al.*, Nature (London) **432**, 203 (2004).
[7] L. Heyne *et al.*, Phys. Rev. Lett. **100**, 066603 (2008).
[8] M. Hayashi *et al.*, Phys. Rev. Lett. **96**, 197207 (2006).
[9] M. Hayashi *et al.*, Appl. Phys. Lett. **92**, 162503 (2008).
[10] D. McGrouther *et al.*, Appl. Phys. Lett. **91**, 022506 (2007).
[11] E. Martinez *et al.*, Phys. Rev. B **77**, 144417 (2008).
[12] M. Kläui *et al.*, Appl. Phys. Lett. **83**, 105 (2003).
[13] S. Lepadatu and Y. B. Xu, Phys. Rev. Lett. **92**, 127201 (2004).
[14] J. C. Slonczewski, J. Magn. Magn. Mater. **159**, L1 (1996).
[15] L. Berger, Phys. Rev. B **54**, 9353 (1996).
[16] G. Tatara and H. Kohno, Phys. Rev. Lett. **92**, 086601 (2004).
[17] S. Zhang and Z. Li, Phys. Rev. Lett. **93**, 127204 (2004).
[18] S. E. Barnes and S. Maekawa, Phys. Rev. Lett. **95**, 107204 (2005).
[19] A. Thiaville *et al.*, Europhys. Lett. **69**, 990 (2005).
[20] A. Yamaguchi *et al.*, Jpn. J. Appl. Phys. **45**, 3850 (2006).
[21] D. Ravelosona *et al.*, Appl. Phys. Lett. **90**, 072508 (2007).
[22] K. Kirk, J. N. Chapman, and C. D. W Wilkinson, Appl. Phys. Lett. **71**, 539 (1997).
[23] K. Miyake *et al.*, J. Appl. Phys. **91**, 3468 (2002).
[24] L. K. Bogart and D. Atkinson, Appl. Phys. Lett. **94**, 042511 (2009).
[25] A. Yamaguchi *et al.*, Appl. Phys. Lett. **86**, 012511 (2005).
[26] L. Néel, Ann. Geophys. **5**, 99 (1949); W. F. Brown, Phys. Rev. **130**, 1677 (1963).
[27] D. Atkinson *et al.*, Nature Mater. **2**, 85 (2003).
[28] D. Atkinson *et al.*, IEEE Trans. Magn. **39**, 2663 (2003).
[29] E. Martinez *et al.*, Phys. Rev. Lett. **98**, 267202 (2007).
[30] M. J. Donahue and D. G. Porter, Interagency Report NISTIR 6376, 1999; http://math.nist.gov/oommf; A. Vanhaverbeke, http://www.zurich.ibm.com/st/magnetism/spintevolve.html.
[31] R. Allenspach, J. Magn. Magn. Mater. **129**, 160 (1994).